

PCCP

Accepted Manuscript



This is an *Accepted Manuscript*, which has been through the Royal Society of Chemistry peer review process and has been accepted for publication.

Accepted Manuscripts are published online shortly after acceptance, before technical editing, formatting and proof reading. Using this free service, authors can make their results available to the community, in citable form, before we publish the edited article. We will replace this *Accepted Manuscript* with the edited and formatted *Advance Article* as soon as it is available.

You can find more information about *Accepted Manuscripts* in the [Information for Authors](#).

Please note that technical editing may introduce minor changes to the text and/or graphics, which may alter content. The journal's standard [Terms & Conditions](#) and the [Ethical guidelines](#) still apply. In no event shall the Royal Society of Chemistry be held responsible for any errors or omissions in this *Accepted Manuscript* or any consequences arising from the use of any information it contains.

1 **Monomolecular adsorption on nanoparticles with repulsive**
2 **interactions: A Monte Carlo Study**

3
4 O. A. Pinto¹, B. A. López de Mishima¹, E. P. M. Leiva², and O. A. Oviedo^{2,*}

5
6 ¹*Instituto de Bionanotecnología (INBIONATEC-CONICET), Universidad Nacional de*
7 *Santiago de Estero, RN 9 Km 1125 Villa el Zanjón, Santiago del Estero, G4206XCP,*
8 *Argentina*

9 ²*Instituto de Fisicoquímica de Córdoba (INFIQC-CONICET), Departamento de*
10 *Matemática y Física de la Facultad de Ciencias Químicas, Universidad Nacional de*
11 *Córdoba, Córdoba X5000HUA, Argentina.*

12 * Corresponding author: o.a.oviedo@unc.edu.ar

13
14 **Abstract**

15 In the present work, we study the adsorption of different monomolecular species on
16 nanoparticles with different sizes and geometries using a Gran Canonical Monte Carlo
17 method. These species are characterized by repulsive lateral interactions between
18 themselves as it take place in the case of the adsorption of partially charged atoms or
19 molecules. Nanosize effects are analyzed in terms of adsorption on edge and facet sites.
20 The energy minimization in these systems comes out as a complex conjugation of
21 repulsive lateral interactions between the adsorbates and attractive interactions of the
22 adsorbates with the nanoparticle. The phenomenon is analyzed as a function of the
23 occurrence of different ordered structures being formed on the surface of the
24 nanoparticle. It comes out that layers with different structures may coexist on different
25 facets of the nanoparticle. Finally, a discussion of the deposition on flat surfaces and in
26 finite systems is given.

27

1 **Keywords:** Adsorption; Nanoparticles; Grand Canonical Monte Carlo; Repulsive
2 Interaction; Nanothermodynamics.

3

4 **1. Introduction**

5 In real surfaces, crystallographic defects such as impurities, dislocations or borders
6 make thermodynamic properties differ from those of flat surface materials [1]. In the
7 nanoworld, this behavior is even more extreme. Nanoparticles (NPs) are systems
8 characterized by a high curvature and a large heterogeneity in interatomic interactions.
9 The latter causes large deviations from the bulk thermodynamic behavior [2,3].
10 Different physical and chemical properties have been found depending on the size and
11 shape of the nanostructure such as diffusivity [4], sintering [5], chemical reactivity [6],
12 melting [7,8] latent heat of fusion [9], magnetism [10] and the under/over potential
13 deposition transition [11,12].

14 The special behavior of systems made of a relatively small number of particles was
15 recognized in the 1960s by Hill [13], who described the basis of the thermodynamics
16 that he called “of small systems.” Hill described in a visionary way how size could
17 affect various thermodynamic properties of these systems. Keeping the pace of “nano
18 times”, this theoretician extraordinarius [14] gave this area of study a new name; he
19 called it nanothermodynamics [15]. A remarkable result of that, is the need to specify
20 the size of the system for a proper (and correct) thermodynamic characterization, so that
21 “small systems” have one more degree of freedom than large ones [13,15,16].

22 In the case of a very large flat surface, the thermodynamic properties of typical lattice
23 gas models such as adsorption isotherms and energy per site do not show size effects.
24 On the contrary, in the case of adsorption on NPs, nanoeffects were reported in several
25 adsorption thermodynamics properties on both using Grand Canonical Monte Carlo
26 (GCMC) simulations [17] and/or analytic approaches [18]. So, it is not hard to consider
27 the size as a new parameter that allows the understanding of adsorption properties at the
28 nanoscale.

29 From the theoretical electrochemical point of view, typical oxidation-reduction
30 voltammetric curves can be obtained through the simulation of ion adsorption on
31 electrodes in the GCMC scheme. Typical current densities in voltammetric curves can
32 be obtained from the derivative of the adsorption isotherms or by computation of the

1 fluctuations of the ad-particles (see Section 2). The electrode potential is related with
2 the chemical potential of the adsorbate, which is the characteristic variable on GCMC
3 simulations. Rikvold has used this scheme to study several experimental systems such
4 as urea on Pt(100) and bisulfate on Rh(111) by ground-state calculations and GCMC
5 simulation [19]. Similar schemes were also used to study the underpotential deposition
6 of Cu on Au(111) in the presence of sulfate [20] and the electrosorption of Br on
7 Ag(100) [21,22].

8 The deposition of ions or capping molecules generally shows repulsive interactions,
9 which induce the formation of ordered structures on two-dimensional substrates such as
10 (100) or (111) faces of metals. For example, in the special case of repulsive first nearest
11 neighbors (NN) interactions, the deposition results in two-ordered structures: the $(\sqrt{3} \times$
12 $\sqrt{3})$ one, where each ad-particle does not have any NN occupied and the $(\sqrt{3} \times \sqrt{3})^*$ one,
13 which only has three of the NN occupied in triangular lattices [23]. The repulsive effect
14 of lateral interactions has been analyzed for bromide adsorption on Ag(100) and sulfide
15 adsorption on Pt(111). Experimental systems were used to adjust parameters within the
16 simulation. Remarkably, a good fit was only possible introducing long range
17 interactions [24,25]. Following with repulsive interactions, the influence of the range
18 and type of lateral interactions in different adsorption geometries has been studied in the
19 case of flat surfaces [26].

20 DFT calculations have been used to reproduce voltammograms for H adsorption on
21 Pt(100) and Pt(111). The authors analyzed the reactions of protons from aqueous
22 solution on Pt surfaces to form adsorbed hydrogen. The results of the model agreed very
23 well with experiment [27].

24 Dynamic information was obtained using Kinetic Monte Carlo (KMC) simulations to
25 study CO oxidation on steeped surfaces of Rh(111) [28] and on the Pt(111)–electrolyte
26 (sulfuric acid) interface [29]. CO oxidation on Pt surfaces has been modeled using
27 Monte Carlo simulations and mean-field theory, to understand the phenomenon of bulk
28 CO electro-oxidation and stripping voltammetry [30].

29 As can be seen from the above paragraphs, no reference has been made to a systematic
30 study of the variation of the adsorption thermodynamic properties in finite surfaces with
31 repulsive interactions. In this respect, the present paper aims to perform the
32 characterization of the thermodynamics of size effects in NPs and its implications for
33 electrochemical measurements. We will consider different degrees of repulsion,
34 emulating systems ranging from anion adsorption to hard steric effects of capping

1 molecules and the different kinds and sizes of NPs. In the case where the distance
2 between NPs becomes small (concentrated NP systems), the effects of confined spaces
3 between two adjacent NPs could become important. These effects are neglected in the
4 present studies.

5 The paper is organized as follows. Section 2 describes the lattice-gas model and some
6 basic definitions. Section 3 shows the results for the thermodynamic behavior obtained
7 from GCMC simulations. Finally, in Sec. 4 the conclusions and future perspectives are
8 given.

10 2. Model and basic definitions

11 In its simplest, most usual form applied to represent infinite surfaces, the lattice-gas
12 (LG) model describes a layer of type-*B* adsorbates on a lattice of type-*A* adsorption
13 sites, where the substrate is assumed to be homogenous. The Hamiltonian of the
14 adsorbed phase is defined by:

$$16 \quad H_{LG} = w_{BB} \sum_{\langle i,j \rangle}^{NNs} c_i c_j + \sum_{i=1}^M (\varepsilon_i - \mu) c_i \quad (1)$$

17
18 where c_i corresponds to the occupation number of the i -th site that takes the value 1, if
19 the site is occupied or 0, if it is empty. w_{BB} is the interaction energy between adsorbates
20 at neighboring sites, μ is the chemical potential and ε_i is the interaction of a single
21 adsorbate with the substrate. The first and second sums on the right side of Eq. (1) run
22 over all B nearest-neighbors (NNs) pairs and all lattice sites (M), respectively. While
23 simulations are usually carried out for a finite network with periodic boundary
24 conditions, the thermodynamic properties are currently evaluated in the limit $M \rightarrow \infty$.
25 In the LG model, the coordination number, *i.e.* quantity of NNs, of each lattice point is
26 not an effective parameter, because adparticles “see” everywhere the same coordination
27 with the substrate and the same number of neighbors. This is clearly an idealization of
28 the surface. Conversely, a real surface has imperfections such as steps, edges, corners,

1 kink, adatoms, etc., which give a distribution of adsorption energies. In these cases, the
 2 surface is considered as a heterogeneous substrate. Thus, the heterogeneity can be
 3 energetic or geometric. The presence of inhomogeneities generally shifts the adsorption
 4 isotherms towards more negative chemical potentials, thus increasing the stability with
 5 respect to that predicted for a perfect surface [31].

6 In the case of NPs, the LG model given in Eq. (1) needs to be adapted, because the
 7 lattice representing the adsorption sites can no longer be considered as a homogeneous
 8 surface. Here, the coordination number of each point becomes a key parameter. To
 9 solve this problem, a modification of the Hamiltonian given in Eq. (1) allows taking
 10 into account this heterogeneity simply assuming an effective interaction w_{AB} :

11

$$12 \quad \sum_{i=1}^M \varepsilon_i c_i = w_{AB} \sum_{i=1}^M N_i c_i \quad (2a)$$

13

14 Then,

15

$$16 \quad H_{NP} = w_{BB} \sum_{\langle i,j \rangle}^{NNs} c_i c_j + w_{AB} \sum_{i=1}^M N_i c_i - \mu \sum_{i=1}^M c_i \quad (2b)$$

17

18 where, as stated above, w_{AB} is a unique parameter representing the average interaction
 19 energy between adparticles and substrate sites and H_{NP} denotes the nanoparticle-
 20 adapted hamiltonian. In fact, w_{AB} is an effective energy per bond. N_i is the
 21 coordination with the substrate, of the i -th site. We emphasize that the present model
 22 involves different kinds of adsorption sites. For example, in the case of an icosahedral
 23 NP, the adsorption sites on facets correspond to hollow sites. On the other hand, the
 24 borders contain bridge adsorption sites and the vertices contain on-top adsorption sites.
 25 Fig. SII of supplementary information shows some snapshots illustrating the different
 26 types of adsorption sites within the present model.

1 By introducing a variable that depends on the coordination number with the substrate
2 via the term $N_i w_{AB}$, it is possible to model different NPs. Then, we can analyze the
3 effect of different shapes and the size in an independent way. As we will see, w_{AB} is a
4 constant, and the heterogeneity will be introduced via the quantity N_i . This definition
5 implies that the effective contribution of i -th site is configuration dependent. Thus, we
6 can introduce information from the NP morphology in the Hamiltonian in Eq. (2b). For
7 example, $N_i = 3$ corresponds to adsorption on a triangular facet (such as (111)-surface)
8 and $N_i = 4$ on a square one (such as (100)-surface). It is important to observe that
9 $1 \leq N_i \leq 9$, because on the surface of a NP there may exist edge and vertex sites with
10 low coordination and also vacant sites with high coordination. For simplicity, we will
11 consider regular NPs.

12 For the present case, we consider a pre-existing substrate, let us say a seed-NP, with
13 given size and geometry at a temperature T and a chemical potential μ . This seed-NP
14 is formed by atoms of type A (so-called substrate), on which the particles of type B are
15 deposited (adsorbate). The decorated NP, that is the seed-NP plus the deposited
16 particles, will be characterized by the numbers of constituent particles, say N_A and N_B .
17 The M adsorption sites for the B particles are located on the surface of the seed-NP.
18 Each site on this surface is assumed to be linked only to its NNs. This defines a sphere
19 of coordination, which depends on the kind of site, the size and the geometry of the NP.
20 The B particles can be linked with B -type particles (lateral NNs) and with A -type
21 particles belonging to the seed-NP. We define two different interaction energies: w_{AB}
22 and w_{BB} for A - B and B - B bonds, respectively. Repulsion between adsorbates is
23 introduced setting $w_{BB} > 0$ and attractive interaction between A and B particles are
24 introduced by $w_{AB} < 0$. Along all this work, we will be referring the energies in units of
25 $k_B T$. In particular, $w_{AB}/k_B T = -3.86$ and $k_B T = 1.0$ are held fixed. A change of $w_{AB}/k_B T$
26 only implies a shift of the curves along the abscissa axis, and would not affect the
27 overall coverage vs chemical potential behavior.

28 The deposition process is simulated by the Monte Carlo technique in the Grand
29 Canonical ensemble using a typical adsorption-desorption algorithm [32,33]. The
30 Metropolis scheme [34] is used to satisfy the principle of detailed balance. A MC Step

1 (MCS) is achieved when each of the M sites has been tested to change its occupancy
2 state. Typically, the equilibrium state can be well reproduced after discarding the first
3 5×10^6 MCS. Then, the next 2×10^6 MCS are used to compute averages. Evaluation of
4 different thermodynamic quantities follows standard procedures, as described below.

5 The mean coverage, θ , is obtained as a simple average of the simulations:

6

$$7 \quad \theta(\mu, T) = \frac{\langle N_B \rangle}{M} \quad (4)$$

8

9 The differential heat of adsorption, q_d , is obtained from [35]:

10

$$11 \quad q_d(\theta) = \frac{\langle H_{NP} N_B \rangle - \langle H_{NP} \rangle \langle N_B \rangle}{\langle N_B^2 \rangle - \langle N_B \rangle^2} \quad (5)$$

12

13 The differential heat of adsorption is a property experimentally accessible by means of
14 thermal desorption spectra. The physical interpretation of this quantity is the energy
15 associated with the removal of a particle from the surface at a given coverage. q_d
16 contains information on the binding energy. Therefore, it could reflect the different
17 adsorption conditions, *i.e.* at terraces, steps, etc. In this way, thermal desorption spectra
18 could be performed to check some of the predictions of the present modeling.

19 While in the present calculations the chemical potential fixed in the Grand Canonical
20 simulation determines the coverage degree, in electrochemical systems, this role is
21 played by the electrode potential. In fact, the electrode potential difference, ΔE , is
22 linearly related to the chemical potential of the B species according to:

23

$$24 \quad \mu = C - ze_0 \Delta E \quad (6)$$

25

1 Where z is the number of electrons transferred in the electrochemical reaction, e_0 is the
2 elemental charge and C is a constant that depends on the activity of B species in
3 solution and the nature of the reference electrode. The physical reason for the minus
4 sign is due to the fact that, in electrochemistry, an increase of the electrode potential
5 will destabilize the adsorbate, since we are taking away their electrons. While the
6 previous argument seems to suggest that some electronic device is necessary to set the
7 potential difference, we have shown in a previous work that this can be achieved by a
8 redox system in the case of free-standing nanoparticles [11,12,16]. Then, the present
9 results may be also of interest for electrochemical systems.

10 An interesting electrochemical property to simulate and compare with experiments is
11 the fluctuation in the number of B -particles on the surface of the NP, so-called
12 compressibility of the adlayer. This quantity is defined as $\beta^{-1}\partial\theta/\partial\mu$ [36] and is
13 proportional to the current measured in a voltammetric experiment. On the other hand,
14 the dimensionless chemical potential $\beta\mu$ is proportional to the electric potential
15 difference applied between working and reference electrodes [24]. Then, $\beta^{-1}\partial\theta/\partial\mu$
16 plotted versus $\beta\mu$ resembles a voltammogram, if the latter was obtained at equilibrium
17 conditions [24,36]. The derivative $\partial\theta/\partial\mu$ can be computed in the Grand Canonical
18 ensemble via the normalized mean square fluctuations:

$$\beta^{-1}\left(\frac{\partial\theta}{\partial\mu}\right)\approx\langle N_B^2\rangle-\langle N_B\rangle^2 \quad (7)$$

22 where $\beta=(k_B T)^{-1}$ and k_B is the Boltzmann constant. Eqs (5) and (7) result from the
23 thermodynamics fluctuation theory [37,38]. We should note that the quantities given in
24 Eqs. (5) and (7) cannot be predicted theoretically. However they can be obtained using
25 computer simulations.

27 3. Results and Discussion

1 Firstly we introduce briefly our work considering adsorption on infinite flat surfaces. In
2 lattice gas models, the deposition on flat surfaces, the adsorption isotherms, its
3 derivative, energy per site, etc. do not show size effects when the size is changed, as
4 long as the system is large enough. This is because the adsorption isotherm involves an
5 intensive property, *i.e.* coverage can be envisaged as a surface density of ad-particles.
6 To illustrate this behavior in the Fig. 1a, adsorption isotherms for square lattice for
7 several lattice sites M are shown. For simplicity we define $\delta E = |w_{BB}/w_{AB}|$, where the
8 only energy changed is $w_{BB}/k_B T > 0$. A flat plateau is observed at half coverage in
9 concordance with the formation of the $c(2 \times 2)$ structure. The inset shows the fluctuations
10 for a square lattice with different numbers of lattice sites M , calculated from Eq. (6),
11 where no shifts are observed with the size of the system. In Fig. 1b the simulations are
12 repeated for triangular lattices. Two broad plateaus are shown in correspondence with
13 the structures formed at $\theta = 1/3$ and $2/3$. As in the previous case, the derivative shown in
14 the inset is size independent.

15 We turn now to consider surfaces defined in a three-dimensional space, like of NPs.
16 Depending on the shape of the NPs under consideration, it comes out that they can be
17 classified into three groups, depending on the nature of the adsorption sites found at
18 their facets and at their edges. In the first group, we include those NPs having one type
19 of adsorption sites at the facets and one type of adsorption sites at the edges. This is for
20 example the case of icosahedral (ICO) NPs, see Fig. 2a, where all the facets exhibit the
21 $\{111\}$ structure and all edges present equivalent adsorption sites. In the second group,
22 we include those NPs having two types of adsorption sites at the facets and one type of
23 adsorption site at the edges. The NPs belonging to this group can be observed in Fig. 2b.
24 Examples of this type are cuboctahedral (CO) NPs, which present two types of facets:
25 $\{111\}$ and $\{100\}$, sharing only one type of edge. Finally, in the third group, we include
26 those NPs having two types of adsorption sites at the facets and two types of adsorption
27 sites at the edges. NPs with the shape of a truncated octahedron (TO) belong to this
28 group, see Fig. 2c.

29

30 3.1. First NPs group

1 We begin describing an ICO NP. The total number of atoms of an icosahedron can be
2 characterized by a natural number “ n ”, which is related to the size of the seed, and to
3 the number of surface sites. For example, if $n=1$, the NP has $N_A=1$ and $M=12$, the
4 smallest value of the number of surface sites. From the energetic point of view, the
5 adsorbate-substrate interaction energies are: w_{AB} for vertex, $2w_{AB}$ for edge and $3w_{AB}$
6 for $\{111\}$ -facet sites. The adsorbate-adsorbate interaction energies are: $5w_{BB}$ for vertex,
7 $6w_{BB}$ for edge and $6w_{BB}$ for facet sites. We consider simulations for a seed-NP with
8 $N_A=1415$ ($n=7$) and $M=492$. Fig. 3 shows the adsorption isotherms (θ versus
9 $\mu/k_B T$) for several δE values. The isotherm changes its shape from a sigmoid to the
10 occurrence of two plateaus, as the lateral repulsion becomes stronger. The plateaus
11 appear at $\theta=1/3$ and $2/3$ and become wider as δE increases. It is important to note
12 that the plateaus show a fine structure, this will be analyzed later. The surface structure
13 generated at the first plateau reminds the $(\sqrt{3}\times\sqrt{3})$ structure found in infinite planar
14 surfaces, where each ad-particle has no NNs occupied. In the second plateau, a
15 $(\sqrt{3}\times\sqrt{3})^*$ structure is formed, where each ad-particle has only the half of its
16 coordination fulfilled. In Fig. 4a, we present the differential heat under the same
17 conditions as those of Fig. 3. Steps are found at the coverages, where the plateaus are
18 formed in the isotherms of Fig. 3. These steps present small arrests, marked with black
19 ellipses, reflecting the fine structure of the plateaus discussed above. These are
20 particularly remarkable in the case of $\delta E=4.0$. The dotted lines indicate the coverages
21 $1/3$ and $2/3$.

22 An interesting property available from the present MCGC simulations is the
23 compressibility. As mentioned before, this is proportional to the current of
24 voltammograms obtained in electrochemical systems, where the current is plotted as
25 function of potential. Fig. 4b shows $\beta^{-1}\partial\theta/\partial\mu$, as a function of $\mu/k_B T$ for the same
26 system as above. The curve for $\delta E=0.5$ shows three small maxima, which correspond
27 to the inflexion points of the isotherms. The fluctuations decrease as the system
28 approaches the coverages where the structures begin to form. On the other hand, the
29 maxima present a sharp shoulder that corresponds to an increase in $\langle\delta(N)^2\rangle$, when the
30 system passes from a disordered to an ordered state. Although the present system is
31 finite, the fluctuations observed resemble the phase transition observed in an infinite

1 system [38]. A similar behavior has also been reported in simulated voltammograms for
2 two-dimensional systems [24]. These sharp shoulders are marked with back arrows in
3 Fig. 4b for $\delta E=4.0$. We now return to the problem of the fine structure observed in the
4 steps of Fig. 3. To understand these features, we study the dependence of the isotherms
5 on the size of the ICO NPs in Fig. 5 for the particular case of $\delta E=10.0$. The sizes
6 considered range from $N_A=147$ ($n=3$) to $N_A=2869$ ($n=9$). It is remarkable that the
7 first plateau presents no fine structure for $n=3, 6$ and 9 but the opposite occurs for $n=4$
8, $5, 7$ and 8 , as it can be better appreciated in the inset of Fig. 5. On the other hand, the
9 second plateau presents a fine structure for all values of n . To understand the
10 phenomenon described above, it is necessary to analyze the role of the edges in the
11 different surface structures. To build a adsorbate ($\sqrt{3}\times\sqrt{3}$) structure, the NPs needs to be
12 commensurate with this structure. Twelve vertices must be empty and the edges must be
13 alternately filled. When this sequence is fulfilled, the ($\sqrt{3}\times\sqrt{3}$) structure forms without
14 defects and the isotherms show a unique plateau at coverage exactly $1/3$ and a unique
15 step at the differential heat. This geometrical situation can only occur in ICO NP where
16 the index “ n ” is a multiple of 3. This is so because the number of adsorption sites at the
17 edge is $n+1$. If a NP does not satisfy this condition, it leads to frustrations, in the sense
18 that all adatoms cannot minimize its number of occupied NNs simultaneously. Fig. SI2
19 of supplementary information shows some snapshots illustrating this geometrical
20 frustration. On the other hand, for the plateau around $\theta\approx 2/3$, we observe several
21 subplateaus for all values of n . The ($\sqrt{3}\times\sqrt{3}$)* structure, which occurs on a 2D triangular
22 lattice, is not possible on an ICO. This is also due to the fivefold coordination of the
23 vertices. This behavior can also be observed in Fig. SI2 (supplementary information),
24 which shows the differential heats for the several values of n . For n multiple of 3, only
25 one step is visible at $\theta=1/3$, but in the other cases multiple steps occur, in agreement
26 with the behavior of the isotherms. In Fig. IS3 (supplementary information), we show
27 an isotherm for a ICO-NP of size equal to $n=9$ with $\delta E=7.0$, an extreme situation
28 (strongly repulsive interaction), where an effective separation of the 3 frustrated states
29 at $\theta=2/3$ can be observed. The previous behavior can be also analyzed taking into
30 account the *average number of links* (Lk), that we define as the average number of
31 occupied neighbors per adsorbate in the NP. For a two-dimensional substrate, the
32 ($\sqrt{3}\times\sqrt{3}$) structure has $Lk=0.0$ for $\theta\leq 1/3$ because no adsorbed particle has occupied
33 NNs sites. The ($\sqrt{3}\times\sqrt{3}$)* structure has $Lk=3.0$ while at full coverage $Lk=6.0$. Fig. 6a

1 shows Lk versus θ for several values of n characterizing the ICO NP. At $\theta < 1/3$ there
2 are practically no links and $Lk = 0.0$ and when the NP is filled $Lk = 5.9$ because the
3 adsorption sites at the vertices are linked with five NNs instead of six. In the zoom of
4 the Fig. 6a, we can observe that for “ n ” non-multiple of three, the curve increases for
5 $\theta < 1/3$, showing that there are particles that are linked with each other at these
6 coverages. This is induced by the geometry of the ICO. The change in the slope of Lk
7 is coincident with each sub plateau observed in the isotherms, (the black lines in the
8 inset are a guide to the eyes). For $n = 3, 6$, and 9 no links are evident for $\theta < 1/3$. In this
9 case, the structure $(\sqrt{3} \times \sqrt{3})$ is completely formed in all the surface of NP, and the links
10 begin to increase for values higher than $\theta = 1/3$. Fig. 6b-d presents the normalized
11 distribution of links (Dis) versus NN, for a ICO of $n = 9$. For a $(\sqrt{3} \times \sqrt{3})^*$ structure, we
12 expect a distribution with a maximum at 3.0 . However in all plateaus we observe sites
13 linked with two, four and five NNs occupied. Thus, plateaus correspond to frustrated
14 $(\sqrt{3} \times \sqrt{3})^*$ structures, something that also becomes evident in the differential heat. Fig. 7
15 shows the simulated voltammograms for different ICO NP sizes. Independent of n , all
16 maxima occur at roughly the same chemical potentials. As expected, in the regions
17 where the plateaus in the isotherm are flat, no evidence for the presence of peaks for
18 $n = 6$ and 9 is found. However, for $n = 7$ and 8 , two new small maxima appear; these
19 correspond to the formation of sub-plateaus related with these frustrated $(\sqrt{3} \times \sqrt{3})$
20 structures. Inset shows a zoom of the first flat region.

21 Now we analyze other NP geometries but within the first group. Under the present
22 approach, the adsorbates on the facets of regular decahedra (DH) and regular tetrahedra
23 (TH) have the same type of repulsive lateral interactions as those of the facets of ICO
24 NPs. The sites on the facets have a lateral coordination of six. The main difference
25 resides in the different relative number of adsorption sites at edges and facets. Sub-
26 plateaus are also present around $\theta = 1/3$ and $2/3$ for values of “ n ” not compatible with
27 the formation of the $(\sqrt{3} \times \sqrt{3})$ structure. Fig. SI4 illustrates this behavior.

28

29 3.2. Second NPs group

30 In this section, we describe the behavior a NP with cuboctahedral (CO) geometry. A CO
31 NP has six $\{100\}$ and eight $\{111\}$ facets. The CO has four types of adsorbate-substrate

1 energies; w_{AB} , $2w_{AB}$, $3w_{AB}$, and $4w_{AB}$ that correspond to adsorption on vertex, edge,
2 $\{111\}$ and $\{100\}$ -facet sites, respectively. It is important to note that all edges
3 connecting $\{111\}$ and $\{100\}$ facets, present the same coordination. Fig. 8a shows
4 isotherms calculated for a CO with $N_A = 2057$, $w_{AB}/k_B T$ was settled like as the ICO and
5 $\delta E = 0.0, 1.0, 2.0$, and 3.0 . As lateral interactions increase, several plateaus are formed.
6 For $\delta E = 0.0$, the calculated isotherm is in agreement with the Langmuir conditions. In
7 the first plateau (*i*) at $\theta \approx 0.40$, the typical structures $c(2 \times 2)$ and $(\sqrt{3} \times \sqrt{3})$ are formed at
8 the $\{100\}$ and $\{111\}$ -facets, respectively. Due to repulsion, all sites prefer not to have
9 any lateral link. Fig. 8b shows a representative snapshot of the CO for this first plateau.
10 The second plateau (*ii*) is formed at $\theta \approx 0.44$. When the vertex sites change their status,
11 there is an inversion in the occupation in the edge sites. This induces a reorganization of
12 the occupation on the $\{111\}$ facet and a complete inversion at the $\{100\}$ facet. It is
13 worth remembering that vertex sites are sites with a higher energy. The $\{111\}$ facet now
14 shows the presence of dimers and trimers, always starting at the edge sites (see Fig.
15 IS5). This corresponds to a new type of frustration; we mean all ad-particles cannot
16 satisfy their energetic requirements. The filling sequences of the edge and vertex sites
17 induce frustration on all NPs. This is shown in the Fig. 8c. There, we show the
18 corresponding snapshot for the (*iii*) plateau at $\theta \approx 0.82$, where the $\{100\}$ -facets are
19 filled, see Fig. 8d. Simultaneously, at the $\{111\}$ facets the structure $(\sqrt{3} \times \sqrt{3})^*$ is formed.
20 The last plateau (*iv*) at $\theta \approx 0.91$ is characterized by the filling of the remaining edge
21 sites. The corresponding snapshot is shown in Fig. 8e. The voltammogram for the
22 present geometry is shown in Fig. IS6.

23

24 3.3. Third NPs group

25 Finally, we consider a truncated octahedron (TO) geometry. Like in the CO, in this
26 geometry there are two different facets: $\{111\}$ and $\{100\}$ (see Fig. 2c). However, in this
27 NP type there are also edge sites of different types, with different coordination numbers:
28 those connecting $\{111\}$ facets with each other and those connecting $\{111\}$ with $\{100\}$
29 facets. Thus, the TO NP has four types of adsorbate-substrate energies; w_{AB} (vertex and
30 $\{111\}$ - $\{111\}$ edges), $2w_{AB}$ ($\{100\}$ - $\{111\}$ edges), $3w_{AB}$ ($\{111\}$ facets), $4w_{AB}$ ($\{100\}$
31 facets) and three types of adsorbate-adsorbate energies; $5w_{BB}$ ($\{111\}$ - $\{100\}$ edges), 4
32 w_{BB} ($\{100\}$ facets), $6w_{BB}$ ($\{111\}$ facets and $\{111\}$ - $\{111\}$ edges). Fig. 9 shows the

1 isotherms for the TO using $N_A = 405, 976, 1925$ and 3348 for $\delta E = 3.0$, here $w_{AB} / k_B T$
2 has the same value as before. The behavior is similar to that of the CO geometry: two
3 principal plateaus are formed. The first corresponds to the case where each particle has
4 no NNs. On the $\{100\}$ and $\{111\}$ facets the structures $c(2 \times 2)$ and $(\sqrt{3} \times \sqrt{3})$ are formed,
5 respectively. In the second plateau, the $\{100\}$ -facets are filled and on the hexagonal
6 facets each particle is linked with other three, forming the $(\sqrt{3} \times \sqrt{3})^*$ structure. For all
7 sizes, the formation of sub plateaus is observed. The insets b) and c) present snapshot of
8 the structures at the first and second plateaus respectively.

9 Fig. IS7a presents the simulated voltammogram for several sizes of TO NPs with the
10 same set of parameters of Fig. 9. Three main maxima are observed, which become
11 better defined as size increases. The sub plateaus in the isotherms appear here as small
12 peaks. The differential heat show steps and sub steps, in correspondence with the
13 behavior of the isotherms as is shown in the Fig. IS7b.

14 NPs pristine with perfect geometries such as those discussed in the previous sections are
15 rarely found in experiments. Surface defects such as adatoms, vacancies and other sites
16 are the generality rather than the exception. It is even possible to find domains with
17 different crystallinities present in the same NP. It is very common to find NPs of
18 different geometries within the same set of synthesized NPs. Despite this complex
19 scenario, is possible to extract valuable information by analyzing the behavior of perfect
20 NPs. For example, Fig. 10 shows the normalized mean square fluctuations as a function
21 of chemical potential at $T = 300$ K for ICO, TH, CO and TO NPs of a similar sizes, such
22 as may be obtained in an experimental histogram. The convolution of all fluctuations
23 shown in the figure can be used to give an idea of "experimental noise" in the
24 voltammograms, caused by different shapes but similar sizes of NPs. For the
25 convolution shown in Fig. 10 we have assumed a population of NPs composed of the
26 same proportions of ICO, TH, CO and TO. The number of sites available on the facets,
27 edges and vertices determine the height of each peak. Then, it is clear that the
28 convolution is not unique. The line in Fig. 10 shows three well defined regions; the first
29 where expanded structures such as $(\sqrt{3} \times \sqrt{3})$, (2×2) and their frustrated structures coexist;
30 the second where expanded and compact structures of type frustrated $(\sqrt{3} \times \sqrt{3})^*$ and
31 (1×1) coexist; and finally a third region where only compact structures coexist. Because
32 the extent of the separation of these three regions exhibits a strong dependence on the
33 magnitude of the repulsion between the adsorbates (as shown qualitatively in Fig. 4), for

1 relatively weak but repulsive interactions, adsorption may yield a broad shoulder in the
2 voltammograms, where all structures coexist simultaneously.

3 In the light of the present results it is interesting to remark the main differences between
4 these nanostructured systems and flat surfaces. Adsorption on flat surfaces does not show
5 size effects for relatively large systems. For example, in 2D lattices the main
6 thermodynamics properties do not change when tend to the thermodynamics limit (
7 $M \rightarrow \infty$). In all cases the ordered structure involved a continuous phase transition for
8 repulsive interactions. Even the related derivatives do not show differences in the
9 intensity or shift of their peaks.

10 In the nanosystems analyzed here, there are a few features such as sites with different
11 coordination on facets, borders, and vertices that play an important role. These features
12 induce the nanoeffects observed. These nanoeffects are manifest in a shift in the
13 isotherms, in the different intensities in the compressibility peaks, etc, at several NP
14 sizes.

15 The repulsive character of the lateral interactions is responsible for the ordered
16 structures formed on the facets. The size of the NP is directly related to the size of each
17 facet and the commensurability of the ordered structures depend on the quantities of
18 adsorption sites. The frustrations and the subplateaus observed are consequences of this.

19

20 **4. Conclusions**

21 In the present work we have studied size and shape effects for the formation of
22 adsorbates presenting repulsive interactions, on the surface of a nanoparticle. Nanosize
23 effects were analyzed, considering adsorption at edge and facet sites within a lattice gas
24 model and Monte Carlo simulations. The energy minimization results from the complex
25 conjugation of repulsive lateral interactions and attractive links between the adsorbates
26 and the seed nanoparticle. Several geometries were considered, emphasizing on
27 icosahedra, cuboctahedra, and truncate octahedra. The properties calculated were
28 adsorption isotherms, differential heats of adsorption, and compressibility with the
29 methods of fluctuations. Depending on the kind of substrate, different types of behavior
30 were found:

- 1 • For icosahedral nanoparticles the $(\sqrt{3} \times \sqrt{3})$ structure is formed on the whole surface
2 only when the index “n” is a multiple of 3. At these indices the NP size is
3 commensurate with this structure. For others values of n, subplateaus are observed
4 in the isotherms in correspondence with frustrations related to the occurrence of the
5 mentioned structure.
- 6 • On the other hand, the $(\sqrt{3} \times \sqrt{3})^*$ structure cannot be completely formed on ICO
7 structures of any size. Then, frustration related to subplateaus are always observed.
- 8 • Compressibility plots show peaks associated with ordered structures, which appear
9 and depending on nanoparticle size.
- 10 • For cuboctahedral nanoparticles, $c(2 \times 2)$ and $(\sqrt{3} \times \sqrt{3})$ or (1×1) and $(\sqrt{3} \times \sqrt{3})^*$
11 structures were formed on the $\{100\}$ and $\{111\}$ facets, respectively. Geometrical
12 frustrations were found too.
- 13 • For truncated octahedral nanoparticles, the existence of $\{111\}$ - $\{111\}$ edges, allow
14 the perfect connection of both $c(2 \times 2)$ and $(\sqrt{3} \times \sqrt{3})$ structures, where no frustration
15 was observed.
- 16 • In two dimensional adsorption phenomena the ordered structures like $c(2 \times 2)$,
17 $(\sqrt{3} \times \sqrt{3})$ and $(\sqrt{3} \times \sqrt{3})^*$ are characterized by order-disorder phase transitions. For
18 each transition, a critical exponent may be determined. These systems have the
19 peculiarity that in the vicinity of criticality the correlation length tends to infinity.
20 This means that in two dimensional lattice-gas models the correlation length reaches
21 the size of the system. Finite size effects are the manifestation of a phase transition
22 and are useful to define the critical temperature. Monomolecular decoration of
23 nanostructures such as nanoparticles or nanoholes is different. A new behavior is
24 observed, corresponding to nano effects. These are manifested in a shift of
25 thermodynamics properties when the size of the nanostructure is changed. These
26 effects tend to hide the size effects associated with the phase transitions taking place
27 on the different facets of the NP. One technique than can help to identify the
28 transition and could allow to obtain the critical temperature is the thermodynamic
29 integration method in the canonical ensemble. With this technique it is possible to
30 analyze the structural disorder in the vicinity of the transition through the
31 calculation of the configurational entropy. In this ensemble other critical functions
32 can be used to help to classify the structural changes found on the surface of NPs.

1 These functions are fourth-order cumulants of energy, order parameters, specific
2 heat, etc. These studies are in progress.

3

4 **5. Acknowledgements**

5 The authors acknowledge financial support from Universidad Nacional de Santiago del
6 Estero, under project CICyT-UNSE 23 A173, CONICET PIP 11220110100992, SECyT
7 Universidad Nacional de Córdoba, Program BID (PICT 2012-2324), and PME: 2006-
8 01581, Argentina.

9

10 **6. References**

11 [1] E. Budevski, G. Staikov, W.J. Lorenz, (1996) Electrochemical phase formation and
12 growth., Wiley-Vch, New York.

13 [2] M. M. Mariscal, O.A. Oviedo, E.P.M. Leiva, (2012) Metal Clusters and
14 Nanoalloys: From Modelling to Applications. Springer Science & Business Media.

15 [3] C. Q. Sun, Size dependence of nanostructures: Impact of bond order deficiency,
16 Progress in Solid State Chemistry, 35, (2007), pp 1-159.

17 [4] S. Horch, H.T. Lorensen, S. Helveg, E. Laegsgaard, I. Stensgaard, K.W. Jacobsen, J.
18 K. Nørskov, F. Besenbacher, Enhancement of surface self-diffusion of platinum atoms
19 by adsorbed hydrogen, Nature 398, (1999), pp 134 -136.

20 [5] S. Mintova, N. H. Olson, V. Valtchev, T. Bein. Mechanism of Zeolite A Nanocrystal
21 Growth from Colloids at Room Temperature, Science 283, (1999), pp 958-960.

22 [6] C.N.R. Rao, G.U. Kulkarni, P.J. Thomas, P.P. Edwards. Size-Dependent Chemistry:
23 Properties of Nanocrystals, Chemistry-A European Journal, 8, (2002) pp 28-35.

24 [7] F. Ercolessi, W. Andreoni, E. Tosati, Melting of small gold particles: Mechanism
25 and size effects, Physical Review Letters 66, (1991), p 7.

- 1 [8] J.P. Borel, Thermodynamical size effect and the structure of metallic clusters,
2 Surface Science 106,(1981), pp 1-9.
- 3 [9] S. L. Lai, J. Y. Guo, V. Petrova, G. Ramanath, L. H. Allen, Size-dependent melting
4 properties of small tin particles: nanocalorimetric measurements. Physical Review
5 Letters, 77 (1996), p 99.
- 6 [10] R.H. Kodama, S.A. Makhlof, A. E. Berkowitz, Finite size effects in
7 antiferromagnetic NiO nanoparticles, Physical Review Letters, 79,(1997) p 1393.
- 8 [11] O.A. Oviedo, E.P.M. Leiva, M.M. Mariscal, Thermodynamic considerations and
9 computer simulations on the formation of core-shell nanoparticles under
10 electrochemical conditions, Physical Chemistry Chemical Physics, 10, (2008), pp.
11 3561-3568.
- 12 [12] O.A. Oviedo, M.M. Mariscal MM, E.P.M. Leiva, On the occurrence of stable and
13 supersaturated metastable states in metallic core-shell nanoparticles, Physical Chemistry
14 Chemical Physics 12 ,(2010), pp 4580-4589 .
- 15 [13] T. L. Hill, Thermodynamics of small systems, Part I and II, Dover. Publication.
16 (1999).
- 17 [14] L. N. Ferguson, Terrell L. Hill Theoretician Extraordinarius, Cell Biochem.
18 Biophys. 11 (1987), pp 11-12.
- 19 [15] T. L. Hill, A different approach to nanothermodynamics, Nano Letters 15 (2001):
20 pp 273-275.
- 21 [16] O.A. Oviedo, E.P.M. Leiva, Thermodynamic Modeling of Metallic Nanoclusters
22 in: M.M. Mariscal, O.A. Oviedo, E.P.M Leiva (Eds.), Metal Clusters and Nanoalloys:
23 From Modelling to Applications. Springer, New York, (2012) p 305.
- 24 [17] O. A. Pinto, B. A. Lopez de Mishima, E. P. M. Leiva, O. A. Oviedo, Computer
25 simulation of adsorption on nanoparticles: The case of attractive interactions, Physical
26 Review E 86, (2012), p 061602.

- 1 [18] O. A. Pinto, B. A. Lopez de Mishima, M. Davila, A. J. Ramirez Pastor, E. P. M.
2 Leiva, O. A. Oviedo, Computer simulation and detailed mean-field approximation
3 applied to adsorption on nanoparticles, *Physical Review E*, **88**, (2013), p.062407.
- 4 [19] E.A. Rikvold, M. Gamboa-Aldeco, J. Zhang , M. Han , Q. Wang , H.L. Richards,
5 A. Wieckowskic, Computational lattice-gas modeling of the electrosorption of small
6 molecules and ions, *Surface Science* 335, (1995), pp 389-400.
- 7 [20] J. Zhang, Y. Sung , P. A. Rikvold, A. Wieckowski, Underpotential deposition of
8 Cu on Au(111) in sulfate-containing electrolytes: A theoretical and experimental study
9 *The Journal of Chemical Physics*, 104,(1996) pp 5699-5712.
- 10 [21] S. J. Mitchell, G. Brown, P. A. Rikvold, Dynamics of Br electrosorption on single-
11 crystal Ag (100): a computational study, *Journal of Electroanalytical Chemistry* 493,
12 (2000): pp 68-74.J.
- 13 [22] I. Abou Hamad, T. Wandlowskic, G. Brown, P. A. Rikvold, Electrosorption of Br
14 and Cl on Ag (100): experiments and computer simulations, *Journal of Electroanalytical*
15 *Chemistry* 554, (2003), pp 211-219.
- 16 [23] A.J. Phares, D.W. Grumbine, F.J. Wunderlich *Langmuir* 23, (2007), pp 1928-
17 1936.
- 18 [24] M. T. M. Koper, Monte Carlo simulations of ionic adsorption isotherms at single-
19 crystal electrodes, *Electrochimica Acta* 446 (1998), pp 1207-1212.
- 20 [25] M. T. M. Koper, A lattice-gas model for halide adsorption on single-crystal
21 electrodes, *Journal of Electroanalytical Chemistry* 450, (1998), pp 189–201.
- 22 [26] M. T. M. Koper, J. J. Lukkien, Modeling the butterfly: influence of lateral
23 interactions and adsorption geometry on the voltammetry at (111) and (100) electrodes.
24 *Surface Science* 498, (2002) pp 105–115.
- 25 [27] G. S. Karlberg, T. F. Jaramillo, E. Skúlason, J. Rossmeisl, T. Bligaard, J. K.
26 Nørskov, Cyclic Voltammograms for H on Pt(111) and Pt(100) from First Principles,
27 *Physical Review Letter* 99, (2007), p 126101.

- 1 [28] T. H. M. Housmans, C. G. M. Hermse, M. T. M. Koper, CO oxidation on stepped
2 single crystal electrodes: A dynamic Monte Carlo study, *Journal of Electroanalytical*
3 *Chemistry* 607, (2007), pp 69–82.
- 4 [29] C. Saravanan, M. T. M. Koper, N. M. Markovic, M. Head-Gordona, P. N. Ross,
5 Modeling base voltammetry and CO electrooxidation at the Pt(111)-electrolyte
6 interface: Monte Carlo simulations including anion adsorption. *Physical Chemistry*
7 *Chemical Physical*, 4,(2002), pp 2660-2666.
- 8 [30] C. Saravanan, N. M. Markovic, M. Head-Gordon, P. N. Ross, Stripping and bulk
9 CO electro-oxidation at the Pt–electrode interface: Dynamic Monte Carlo simulations,
10 *Journal of Chemical Physics*, 114,(2001), pp 6404-6412.
- 11 [31] M. C. Giménez, M. G. Del Pópolo, E. P. M. Leiva, Monte Carlo simulation for the
12 formation and growth of low dimensionality phases during underpotential deposition of
13 Ag on Au (100), *Electrochimica acta*, 45, (1999),pp 699-712.
- 14 [32] K. Binder, D. Stauffer, (1984) Applications of the Monte Carlo Method in
15 *Statistical Physics*, in: K. Binder (Ed.), Springer, Berlin.
- 16 [33] K. Kehr, K. Binder, (1987) “Simulation of diffusion in lattice gases and related
17 kinetic phenomena”, in: K. Binder (Ed.), “Applications of the Monte Carlo Method in
18 *Statistical Physics*”, *Topics in Current Physics*, vol. 36, Springer, Berlin, 181.
- 19 [34] N. Metropolis, A. W. Rosenbluth, M. N. Rosenbluth, A. H. Teller, E. Teller,
20 Equation of state calculations by fast computing machines, *The journal of chemical*
21 *physics* 21, (1953), pp 1087-1092.
- 22 [35] D. Nicholson, N.G. Parsonage, “Computer Simulation and the Statistical
23 *Mechanics of Adsorption*”, Academic Press, London, (1982).
- 24 [36] G. Brown, P. A. Rikvold, S. J. Mitchell, M. A. Novotny, (1999) Monte Carlo
25 methods for Equilibrium and Nonequilibrium problems in Interfacial Electrochemistry
26 in: A. Wieckowski (Ed.), *Interfacial electrochemistry, Theory, Experiment, and*
27 *Applications*, Marcel Dekker, New York.

- 1 [37] M. E. J. Newman, G. T. Barkema, Monte Carlo Method in statistical physics,
- 2 Clarenton –Press Oxford, (1999).

- 3 [38] H. B. Callen, “Thermodynamics and an introduction to thermostatics”, John
- 4 Wiley and Sons, (1985).

1 7. Figures Caption

2 Figure 1: Adsorption isotherms on flat surfaces, for several quantities of adsorption sites
3 M. a) Square lattices, b) Triangular lattices. The respective inset shows the
4 corresponding derivative.

5 Figure 2: (Color online) Representative pictures of nanoparticles presenting: a) one type
6 of adsorption site at the facets and one type of adsorption site at the edges, in this case
7 an icosahedron, b) two types of adsorption sites at the facets and one type of adsorption
8 site at the edges, in this case a cuboctahedron, and c) two types of adsorption site at the
9 facets and two types of adsorption site at the edges, in this case a truncated octahedron.
10 Red lines denote edges. The facet types are marked at each structure.

11 Figure 3: (Color online) a) Adsorption isotherms obtained for an icosahedral NP made
12 of 1415 type-A particles, for several δE values as indicated.

13 Figure 4: (Color online) Results from GCMC simulations for the adsorption of particles
14 with repulsive interactions on an icosahedral NP of 1415 type-A particles. a)
15 Differential heat as a function of coverage degree and b) normalized mean square
16 fluctuations as a function of chemical potential. The parameters of the simulations are
17 the same as those of Figure 3.

18 Figure 5: (color online) Dependence of the isotherm on the size of an icosahedral NP, n ,
19 for $\delta E = 1.0$. The inset shows a zoom of the first plateau.

20 Figure 6: (color online) a) average number of links versus coverage for several values of
21 n charactering the size of the icosahedron. The vertical lines indicate the coverages $1/3$
22 and $2/3$, and the horizontal indicates $Lk = 3.0$. The inset shows a zoom around $\theta = 1/3$.
23 The normalized distribution of links (Dis) for $n=9$ is shown on the right for different
24 coverage degrees, b) $\theta = 0.645$ c) $\theta = 0.667$ and d) $\theta = 0.6889$.

25 Figure 7: (Color online) Fluctuations obtained as a function of the normalized chemical
26 potential for icosahedral NPs of different sizes.

27 Figure 8: (Color online) a) Adsorption isotherms on a CO with $N_A = 2057$ and several
28 values of δE . The plateaus are labeled with “ i ’s”. Snapshot of the representative

1 configurations at the plateaus, the black circles denote occupied sites and the colors are
2 empty sites: b) plateau *i*, c) plateau *ii*, d) plateau *iii* and e) plateau *iv*.

3 Figure 9: (Color online) a) Isotherms obtained for Truncated Octahedra using different
4 values of n , with $\delta E = 3.0$. a) and b) present snapshots of the structures obtained at the
5 first and second plateaus respectively.

6 Figure 10: (Color online) Mean square fluctuations(MSF) as a function of chemical
7 potential for ICO(2057), TH(1771), CO(2057) and TO(1925) NPs at 300 K. The full
8 line is a convolution of the MSF of the four types of NPs with the same weight.

Figure 1

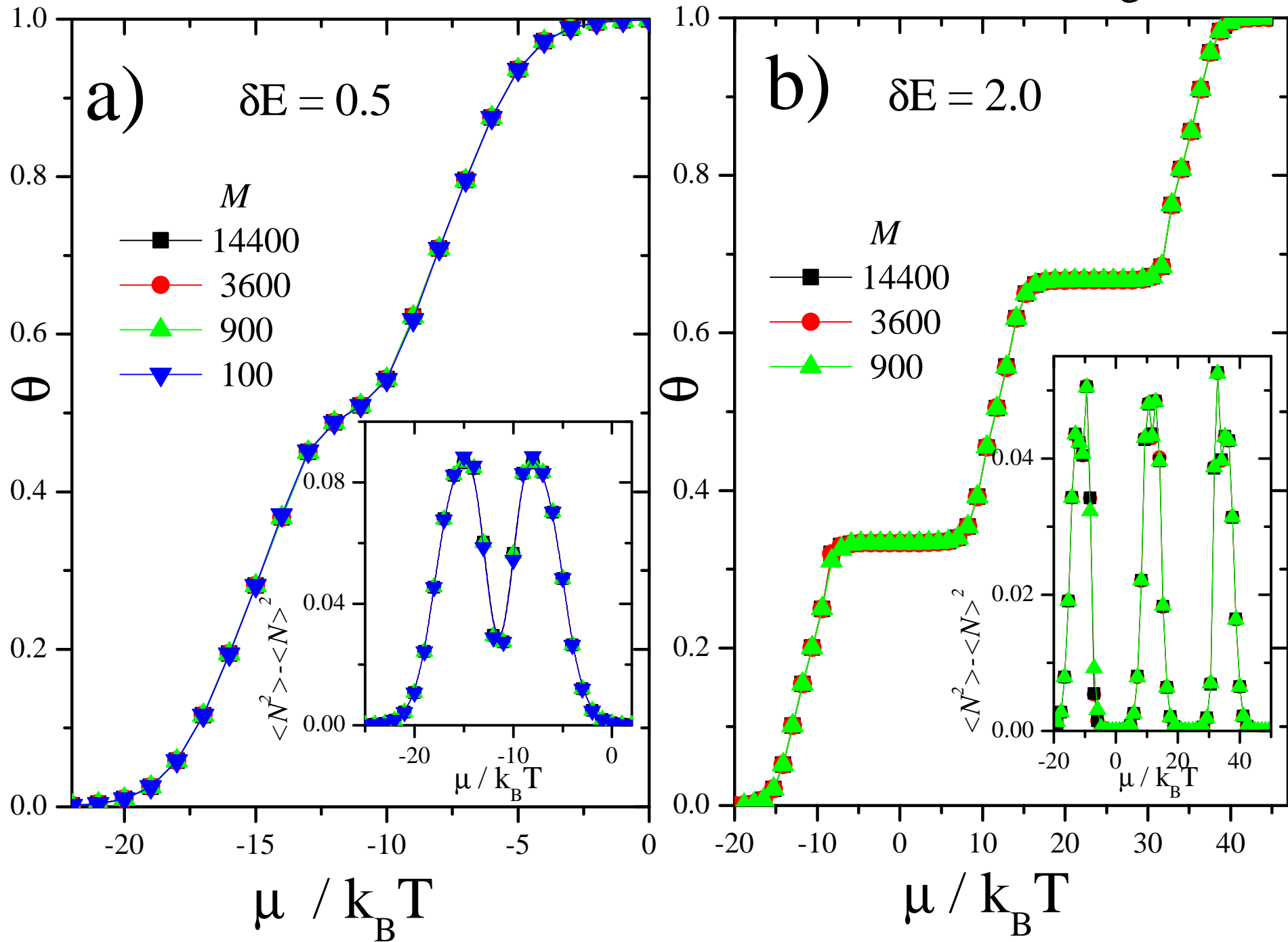


Figure 2

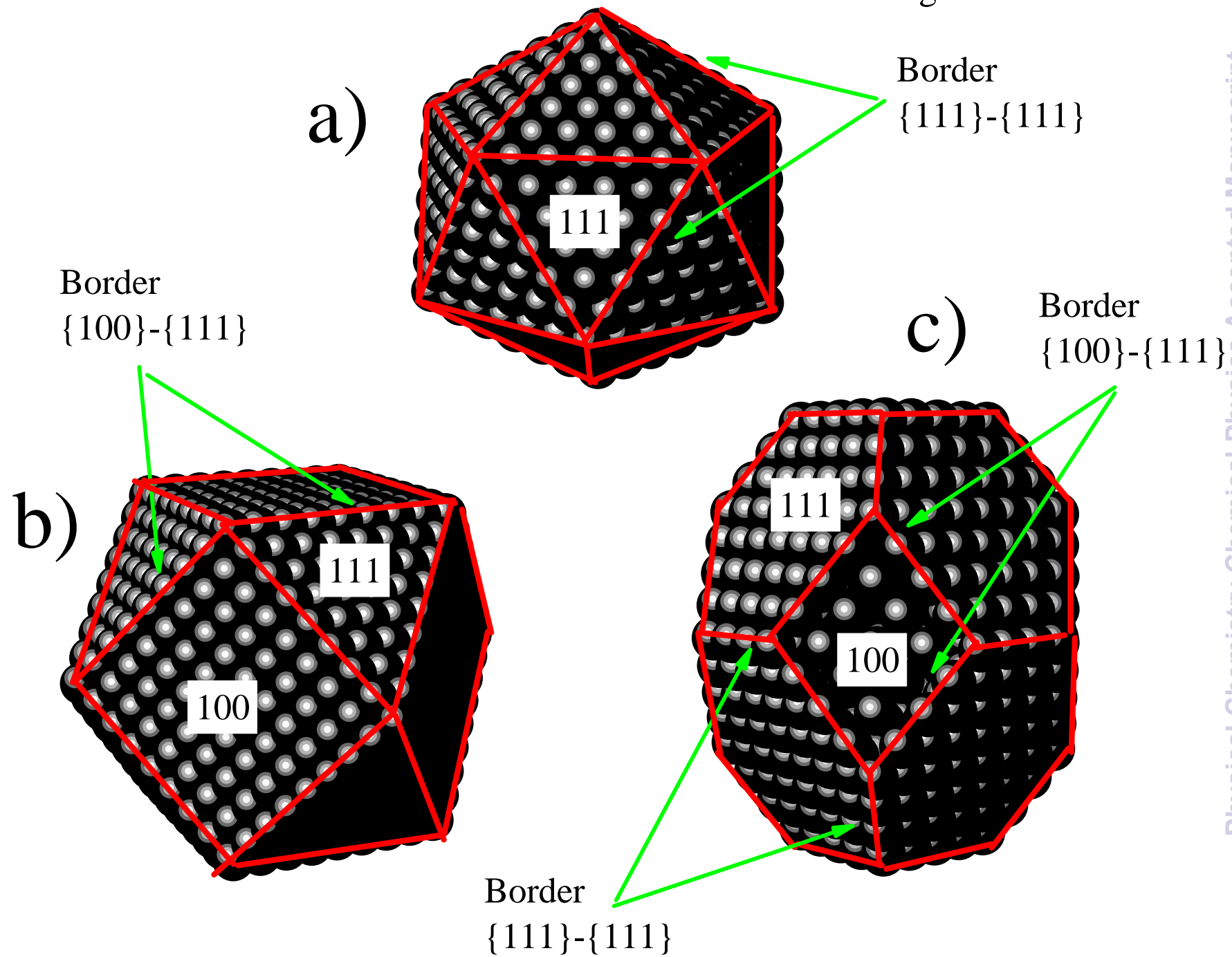
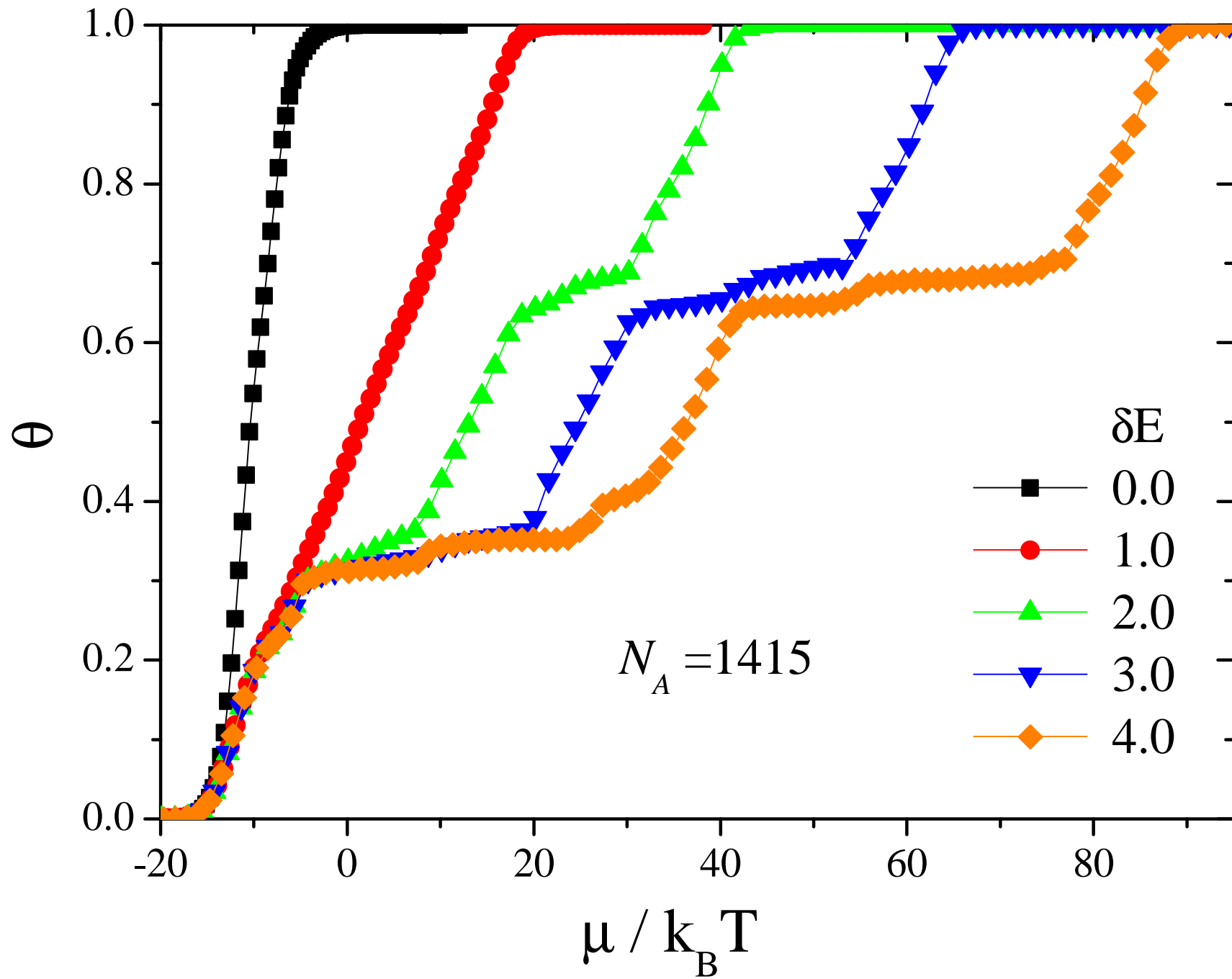


Figure 3



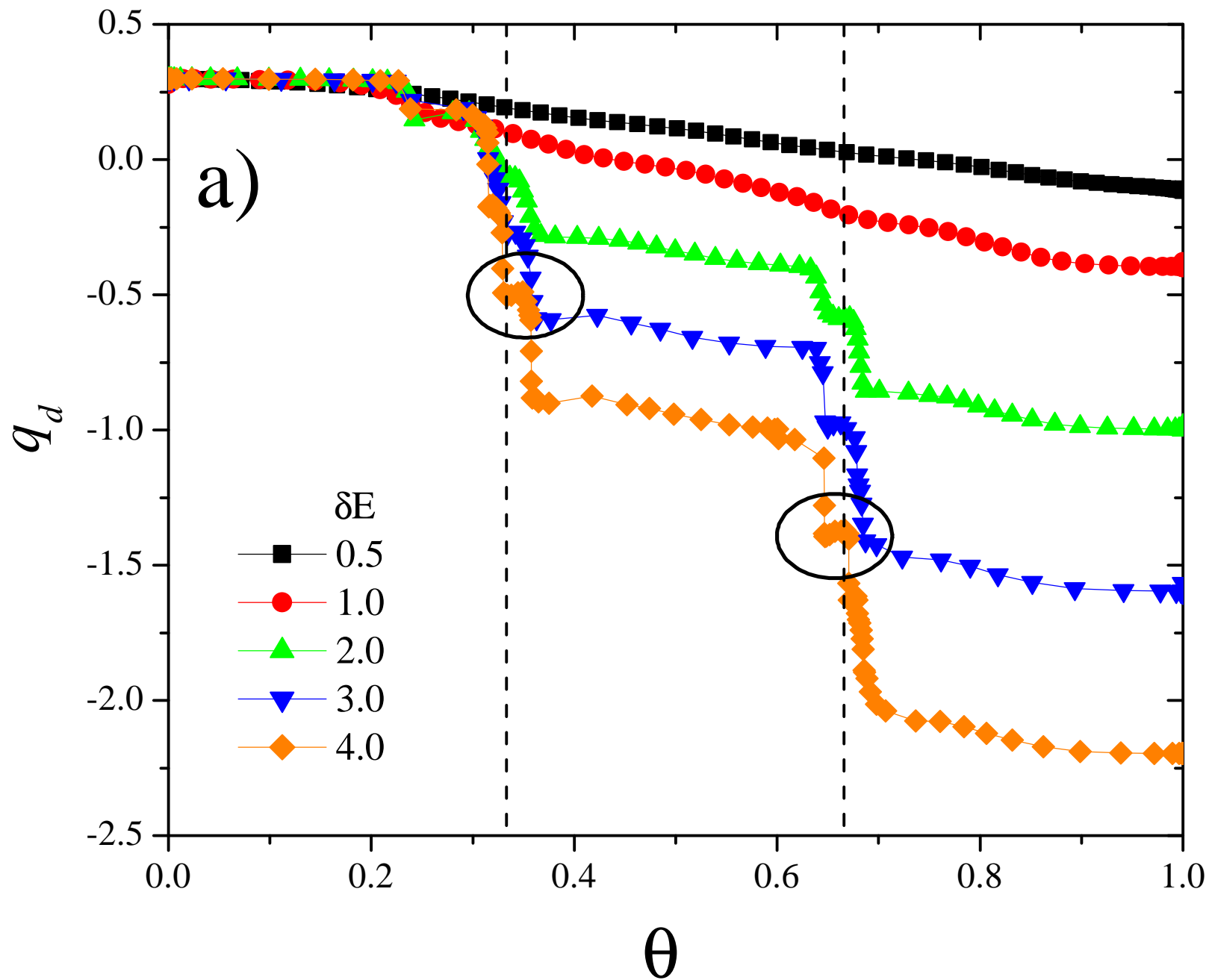


Figure 4b

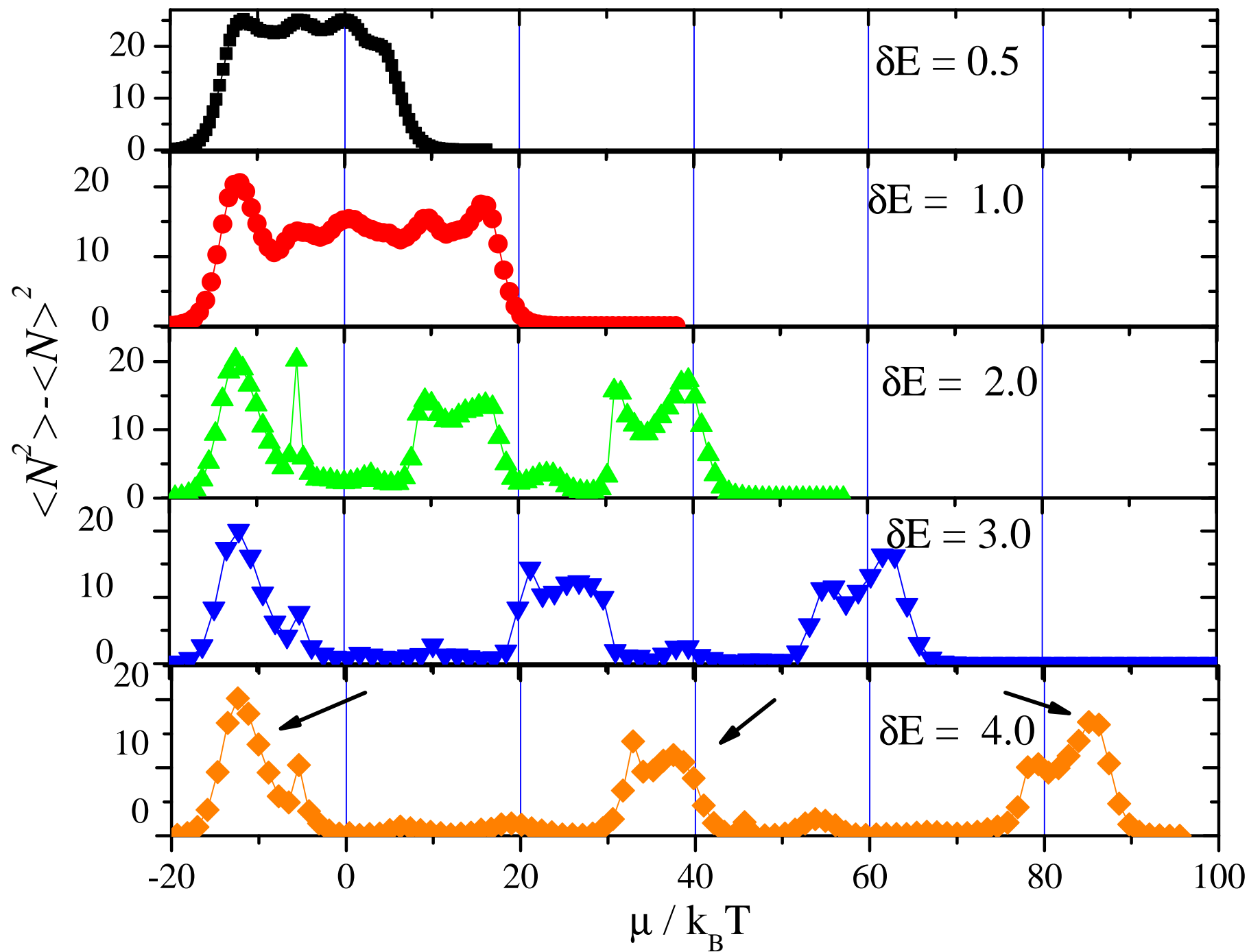
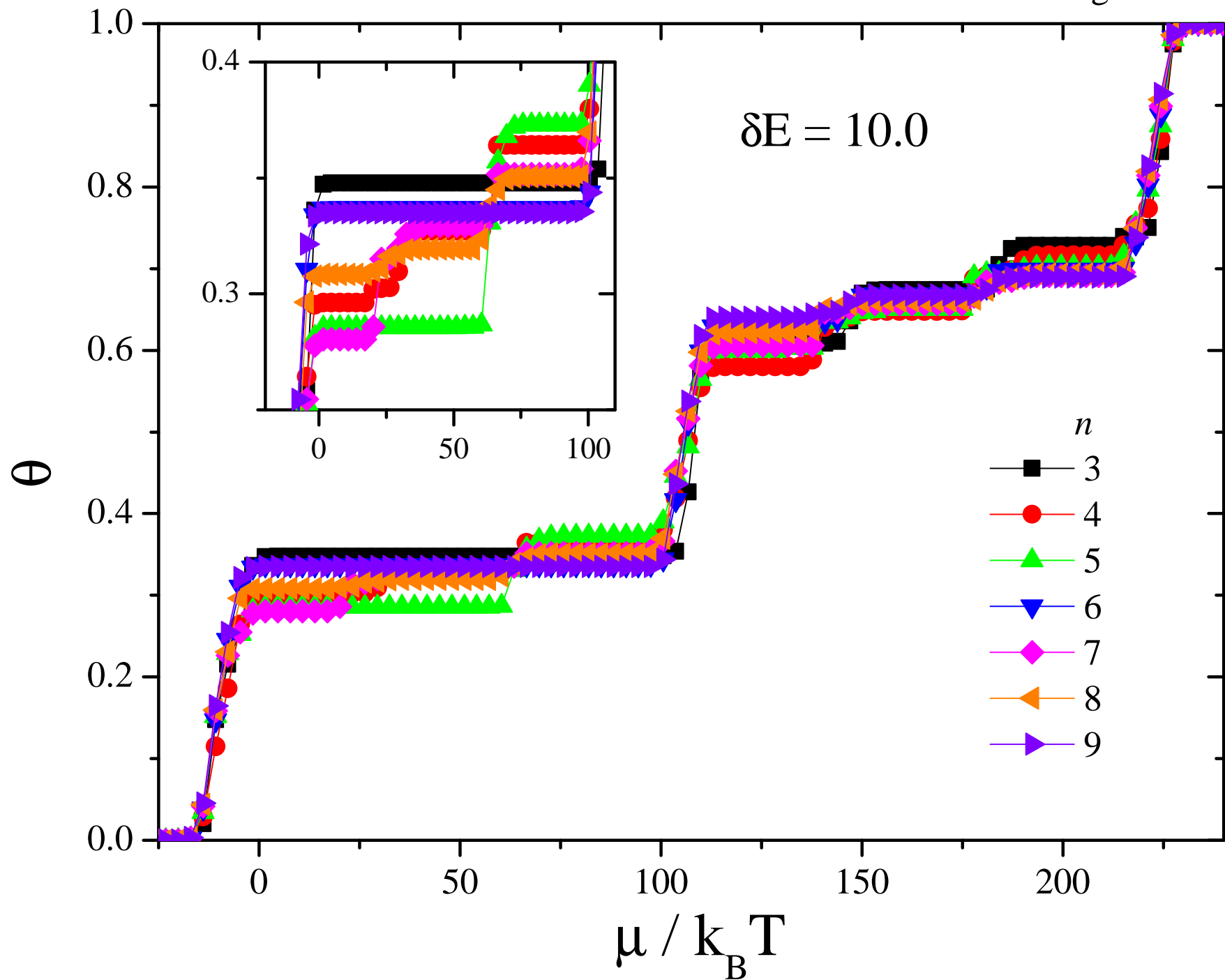
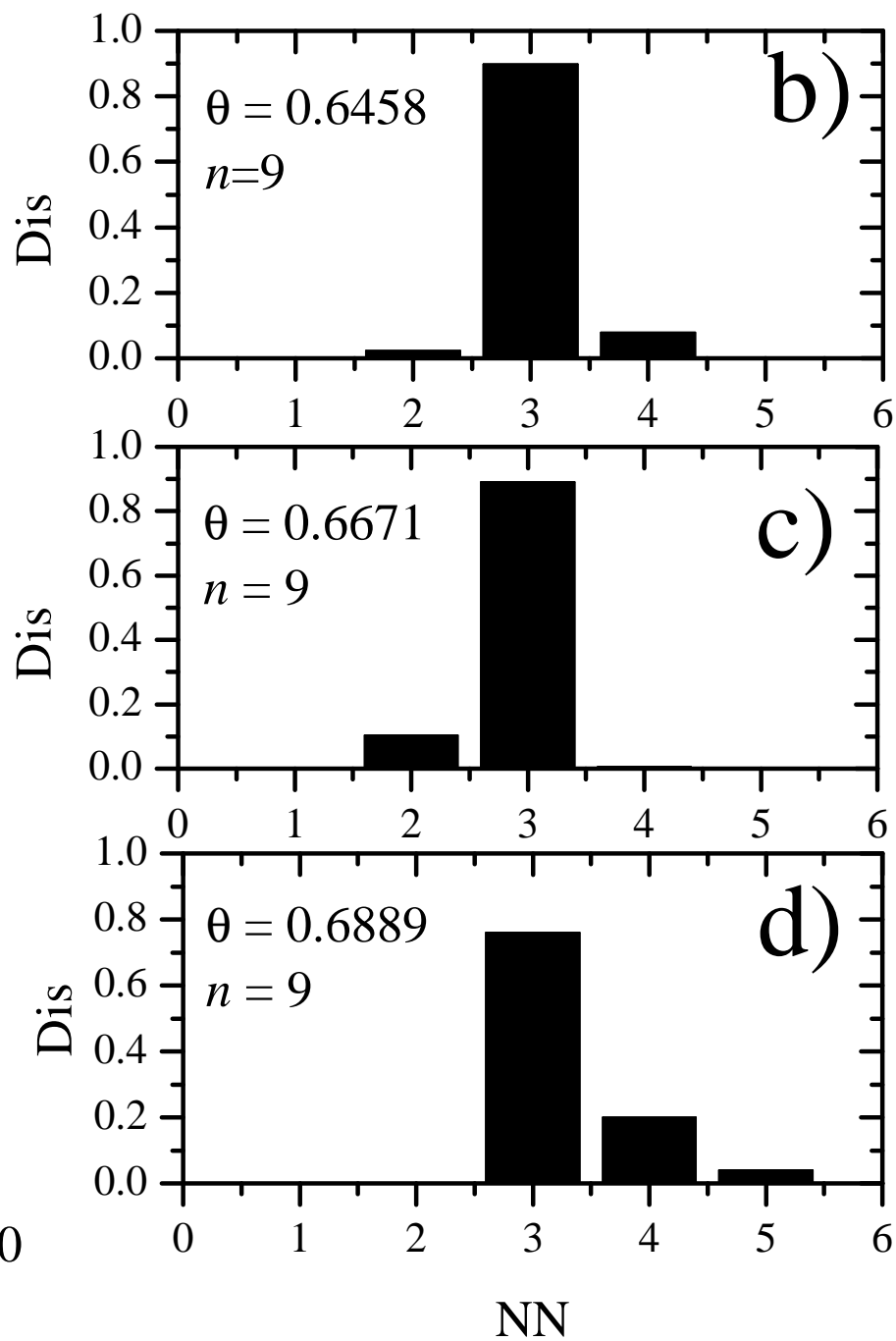
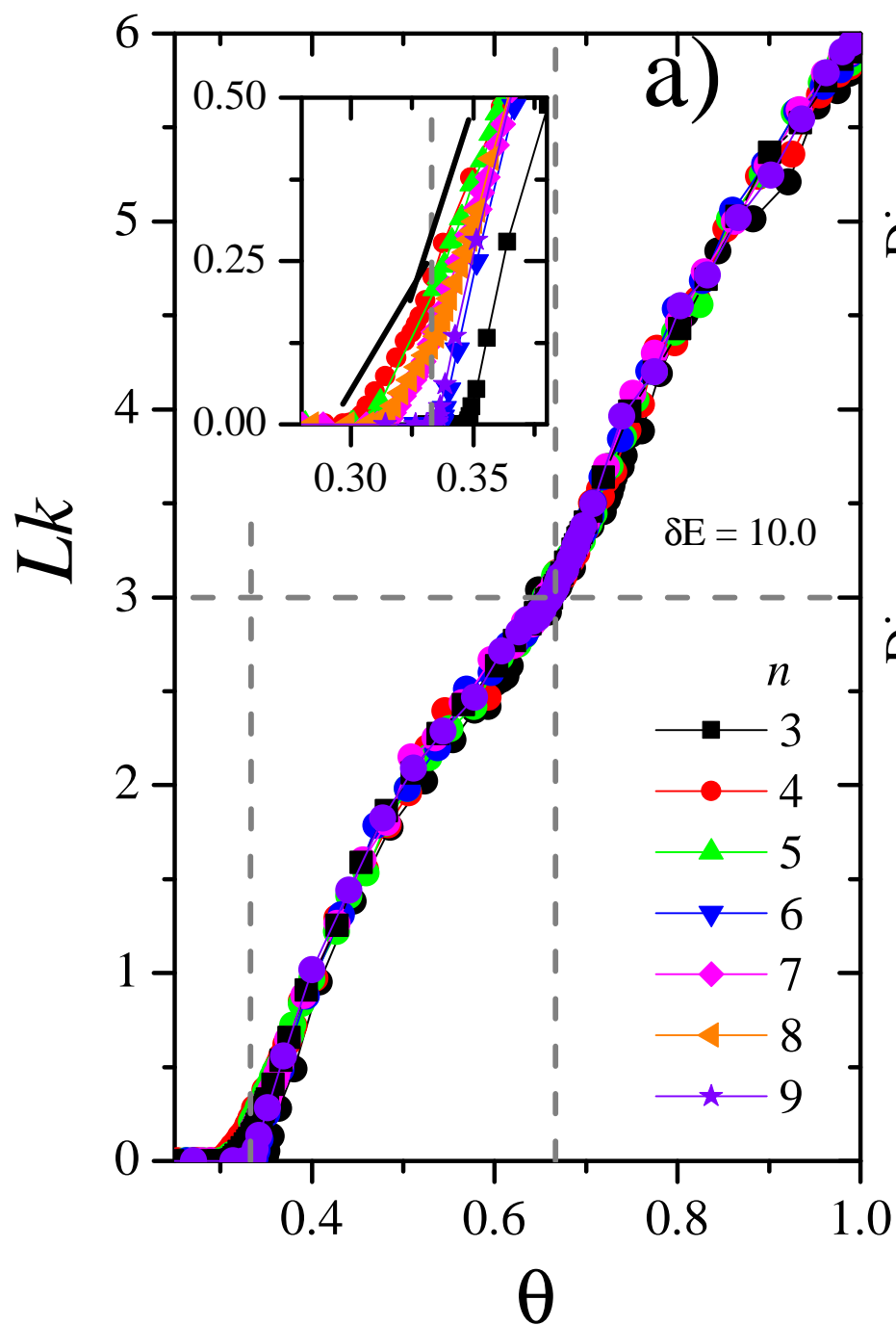
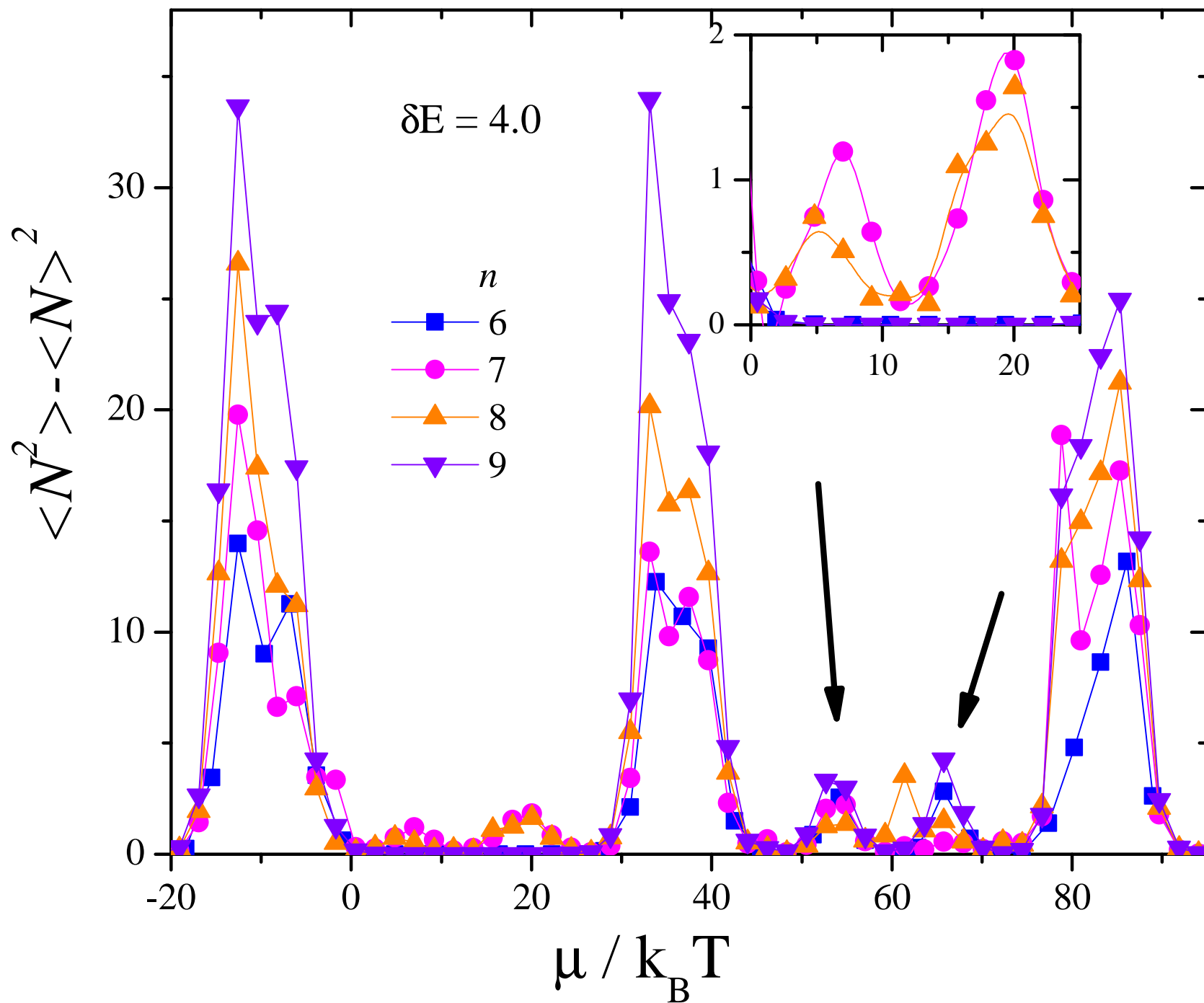


Figure 5







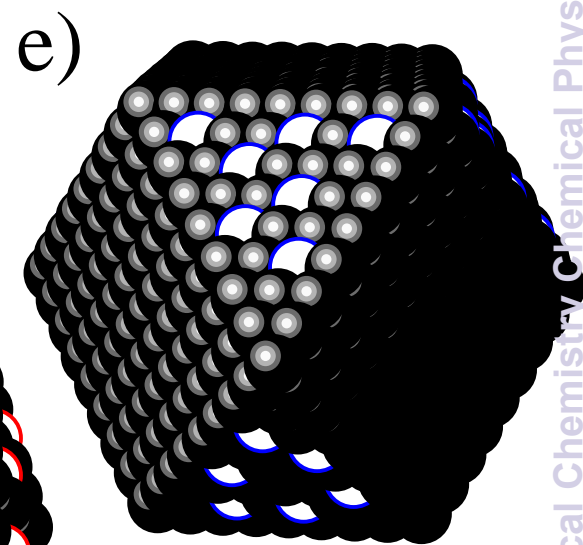
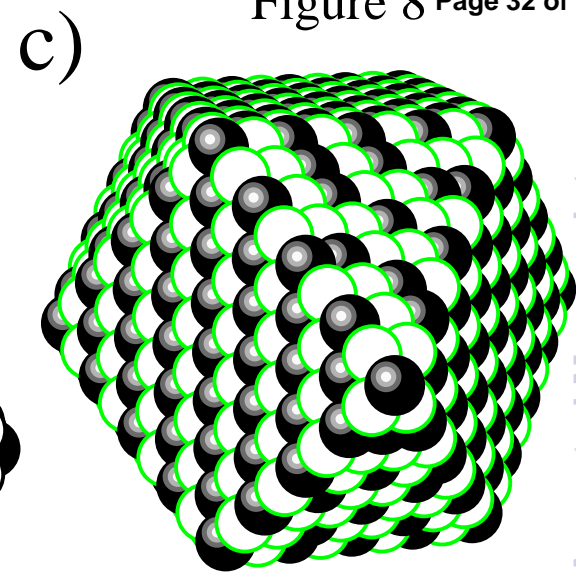
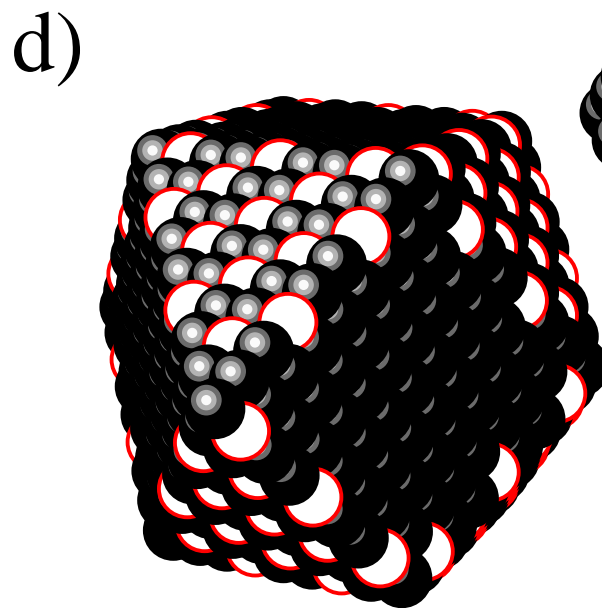
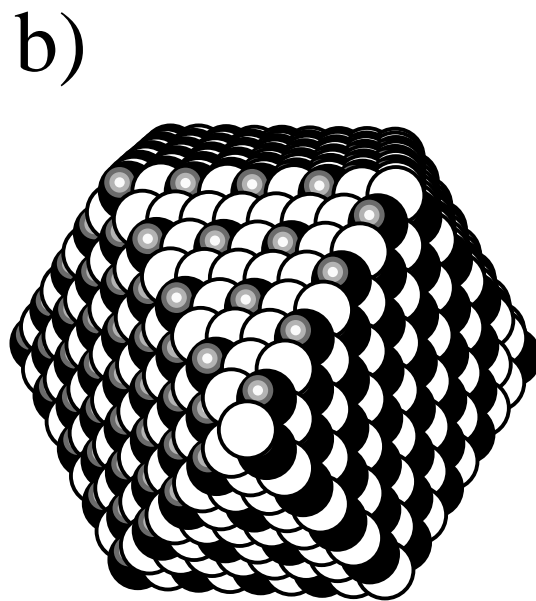
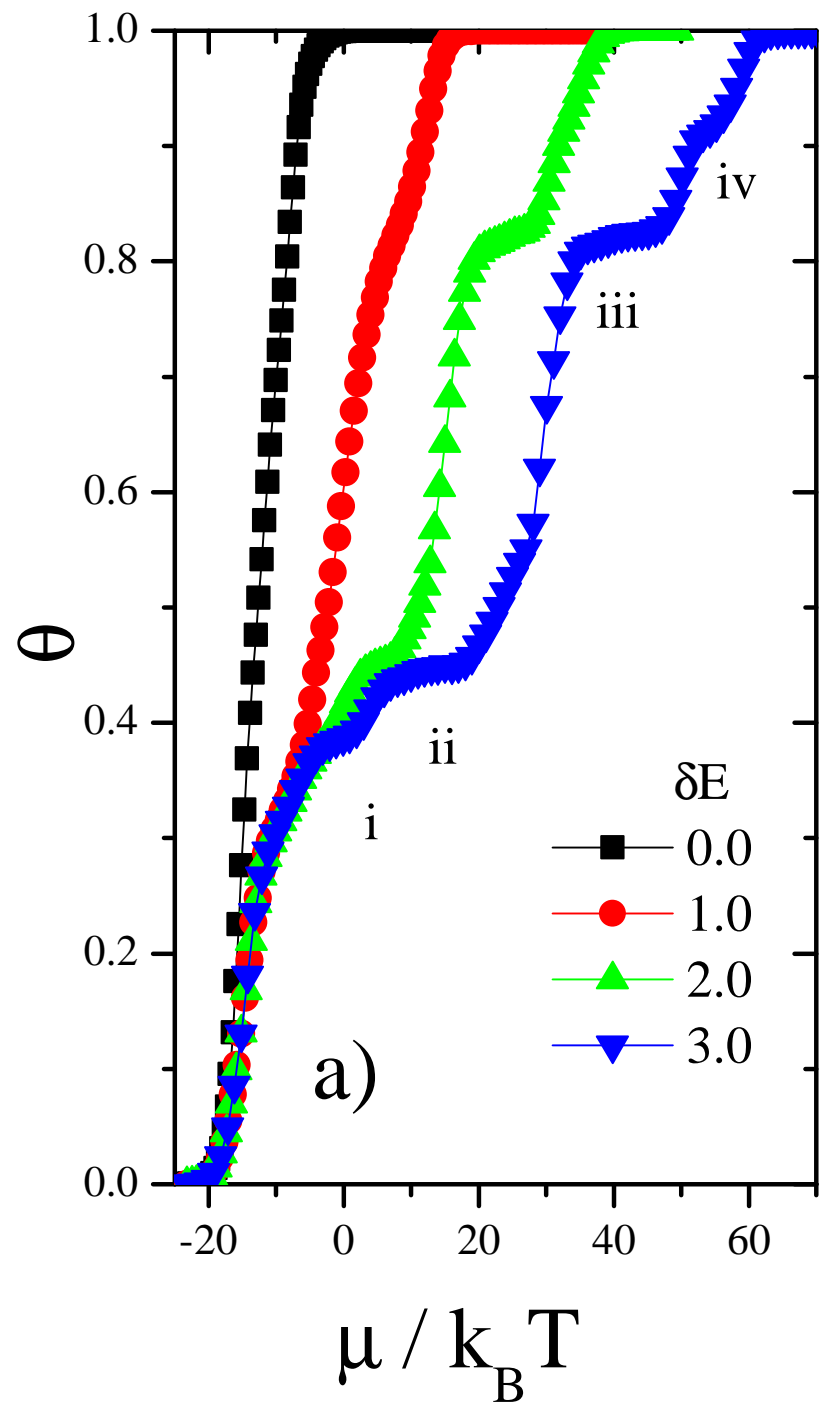
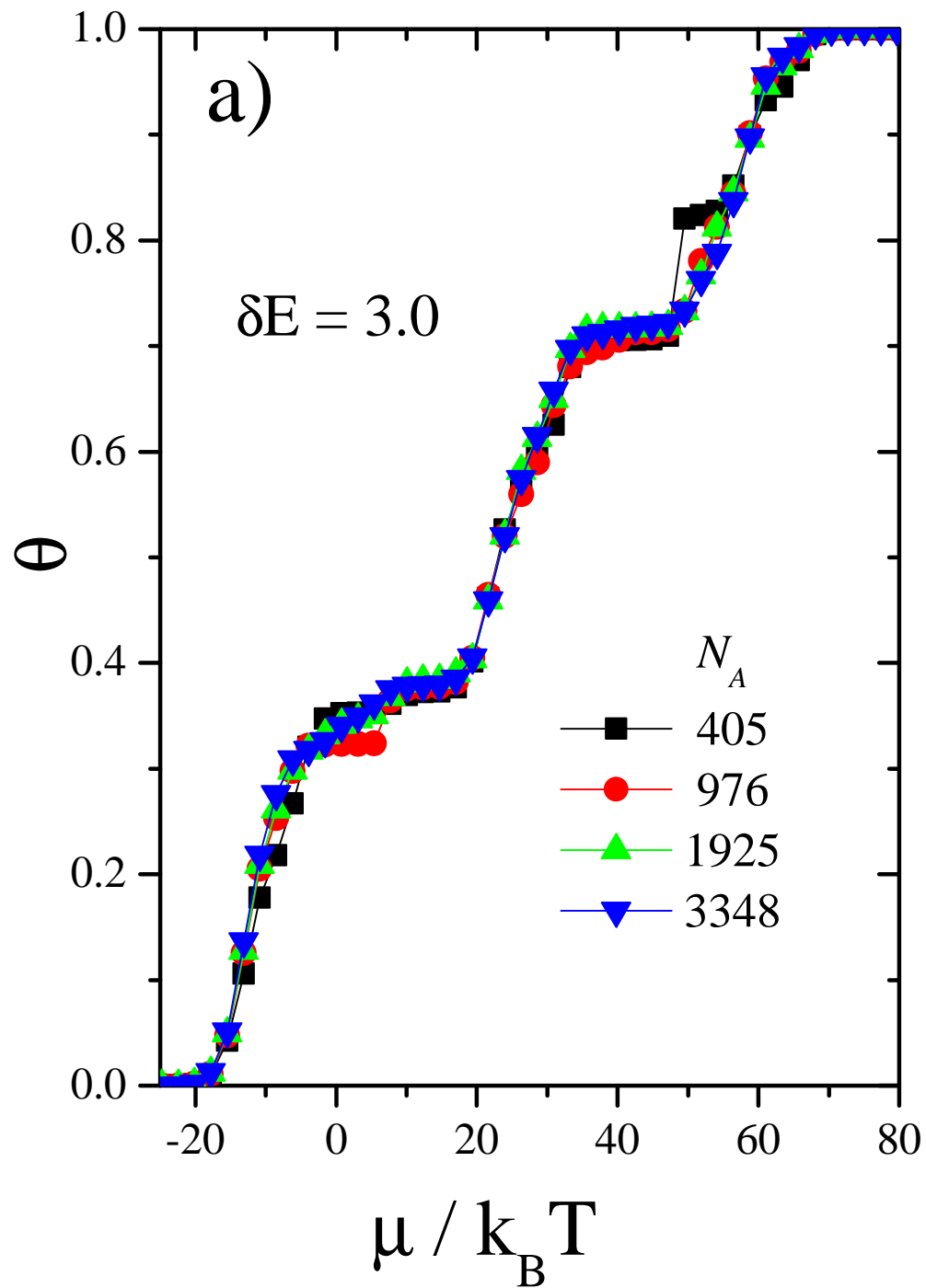
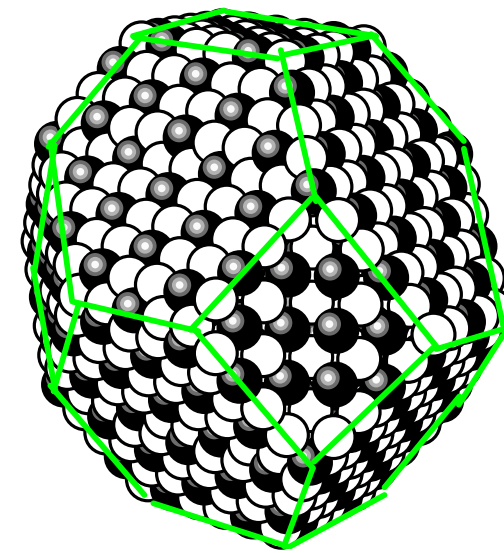


Figure 9



b)



c)

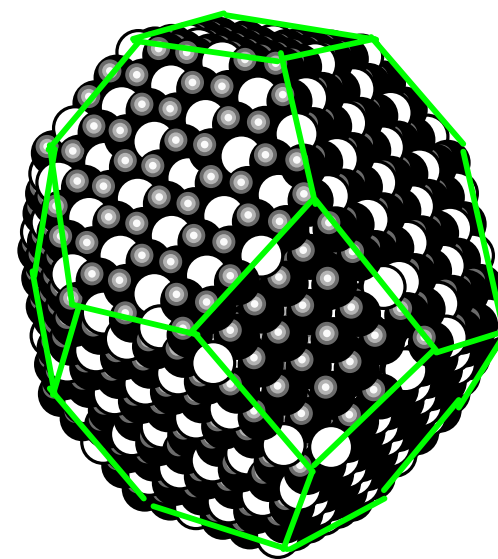


figure 10

